7

Using a Linear Damper

… in which root locus plots are used to explore the impact of a single damper with two different feedback signals and locations of transfer function zeroes in power systems are predicted using the spring-mass inter-area mode model.

The mode controllability and mode observability measures given in Chapters 3 and 4 indicate where to place the actuator and where to measure the selected signal. In this chapter, the loop is closed and the gain of the controller is chosen for maximum damping of selected modes.

The power system with one damper installed can be described as a single-input single-output (*SISO*) system with a feedback controller. The controller output is active power injection at the damper location, and the controller input is either local bus frequency or rotor frequency of the closest machine. With these measurement signals, the controller will be a simple static gain. If instead angles are measured, the controller will include a lead filter with approximately 90° phase advancement at frequencies below a few Hertz. Whenever possible the analysis will consider frequencies as measured directly.

Mode controllability and mode observability supply information that is valuable for suggesting a suitable controller structure, but it is valid only at zero gain. To explore the behaviour of a SISO system for gains greater than zero the *root locus* method is adequate and is used in the instructive PSS article [Larsen and Swann 1981]. The root locus is the path of the system eigenvalues as the gain is varied from zero to infinity. Considering damping of a certain mode, optimum gain is selected as the one that produces maximum damping. The relationship to the previous measures is close since the eigenvalue sensitivity supplied by the mode controllability and mode observability provides the gradient at the starting point of the root locus.

Often a root locus does not need to be traced out in detail to be sufficiently informative. An approximate sketch can be produced by applying a number of rules. According to one of these rules, eigenvalues move towards

transfer function zeroes. If a zero is located at infinity, the eigenvalue will approach along an asymptote, that can be determined by another rule.

The attraction of eigenvalues to zeroes plays a critical role by reducing the control authority. Unfavourably located zeroes thus limit the maximum damping. Consequently, understanding how zeroes arise and what governs their locations is very valuable. This is studied in Section 7.1 by computing the zeroes of the spring-mass inter-area mode equivalent subjected to feedback from the different signals. Section 7.2 treats Multi-Modal Decomposition, which is a model structure that improves the understanding of transfer function zeroes that arise when trying to damp electro-mechanical modes of power systems. In Section 7.3 and 7.4 a damper is introduced in the three and twenty-three machine systems respectively. Root locus plots are shown for the two different feedback signals and optimum gains are selected. Section 7.5 concludes the chapter.

7.1 System Zeroes of the Spring-Mass Model

In accordance with the root locus rule mentioned above the zeroes can be determined as the system eigenvalues for the case with infinite feedback gain. This can be shown by assuming an open loop system with input u and output y corresponding to Laplace transforms $U(s)$ and $Y(s)$. The transfer function of the system is,

$$\frac{Y(s)}{U(s)} = \frac{Z(s)}{P(s)}$$

Introducing the proportional control law,

$$U(s) = K\left[U_{ref}(s) - Y(s)\right]$$

yields a transfer function from reference $U_{ref}(s)$ to output $Y(s)$ as,

$$\frac{Y(s)}{U_{ref}(s)} = \frac{KZ(s)}{P(s) + KZ(s)}$$

where an infinite gain K turns the roots of $Z(s)$ into the eigenvalues of the system. If n_p and n_z are the degrees of the polynomials $P(s)$ and $Z(s)$, n_p is assumed to be greater than n_z and n_p-n_z zeroes are infinite.

Zeroes for Feedback from Local Bus Frequency

Feedback from local bus frequency to active power is introduced in the spring-mass inter-area mode equivalent of Fig. 2.10 by letting the force F_3 depend on the time derivative of x_3 as,

$$F_3 = d_3 \dot{x}_3$$

This only requires d_3 to be inserted as an element of the diagonal matrix in (2.29),

$$diag\left(\begin{bmatrix} M_1 \\ M_2 \\ 1 \\ 1 \\ d_3 \end{bmatrix}\right)\frac{d}{dt}\begin{bmatrix} v_1 \\ v_2 \\ x_1 \\ x_2 \\ x_3 \end{bmatrix} = \begin{bmatrix} 0 & 0 & -k_1 & 0 & k_1 \\ 0 & 0 & 0 & -k_2 & k_2 \\ 1 & 0 & 0 & 0 & 0 \\ 0 & 1 & 0 & 0 & 0 \\ 0 & 0 & k_1 & k_2 & -(k_1+k_2) \end{bmatrix}\begin{bmatrix} v_1 \\ v_2 \\ x_1 \\ x_2 \\ x_3 \end{bmatrix} + \begin{bmatrix} 1 & 0 \\ 0 & -1 \\ 0 & 0 \\ 0 & 0 \\ 0 & 0 \end{bmatrix}\begin{bmatrix} F_1 \\ F_2 \end{bmatrix} \quad (7.1)$$

Note that the model order is increased by one as x_3 is turned from an algebraic variable into a dynamic state. The diagonal matrix can now be inverted and premultiplied from the left.

An infinite gain d_3 causes the time derivative of x_3 to be zero. As x_3 is the output of an integrator with zero input it yields an eigenvalue at the origin and thus the first zero,

$$z_1 = 0$$

As x_3 cannot vary, it will not affect system dynamics and can therefore be treated as a (constant) input. The remaining zeroes are thus obtained as the eigenvalues of the system,

$$diag\left(\begin{bmatrix} M_1 \\ M_2 \\ 1 \\ 1 \end{bmatrix}\right)\frac{d}{dt}\begin{bmatrix} v_1 \\ v_2 \\ x_1 \\ x_2 \end{bmatrix} = \begin{bmatrix} 0 & 0 & -k_1 & 0 \\ 0 & 0 & 0 & -k_2 \\ 1 & 0 & 0 & 0 \\ 0 & 1 & 0 & 0 \end{bmatrix}\begin{bmatrix} v_1 \\ v_2 \\ x_1 \\ x_2 \end{bmatrix} + \begin{bmatrix} 1 & 0 & k_1 \\ 0 & -1 & k_2 \\ 0 & 0 & 0 \\ 0 & 0 & 0 \end{bmatrix}\begin{bmatrix} F_1 \\ F_2 \\ x_3 \end{bmatrix}$$

This gives

$$z_2 = z_3^* = j\sqrt{\frac{k_1}{M_1}};\ \ z_4 = z_5^* = j\sqrt{\frac{k_2}{M_2}} \quad (7.2)$$

where * denotes complex conjugate. For an infinite gain, the system can be viewed as two independent spring-mass systems, with separate resonance frequencies. The four last zeroes are thus the mechanical resonances of the system as the position x_3 is fixed. This agrees perfectly with the result of

[Miu 1991], that "*complex conjugate zeros are the resonant frequencies of a substructure constrained by the sensor and actuator*". Note that whereas the original system had one oscillatory mode, the system with infinite feedback has two, as the rigid body mode is made oscillatory. The zero z_1 at the origin reflects the fact that x_3 can take any value.

From (7.2) the location of the zeroes relative to the eigenvalues of the uncontrolled system is not evident, yet of great interest. Let

$$\frac{k_1}{M_1} = \gamma \frac{k_2}{M_2} \tag{7.3}$$

where γ is a real number. The eigenvalues in (2.30) of the inter-area mode for the uncontrolled system can now be described as,

$$\lambda_1 = \lambda_2^* = j\sqrt{\frac{k_1}{M_1}\frac{M_1+M_2}{\gamma M_1+M_2}} = j\sqrt{\frac{k_2}{M_2}\gamma\frac{M_1+M_2}{\gamma M_1+M_2}}$$

It is now clear that a γ greater than one yields,

$$|z_4| < |\lambda_1| < |z_2|$$
$$|z_5| < |\lambda_2| < |z_3|$$

which is illustrated in the left graph of Fig. 7.1. A γ less than one gives the opposite relations, but looks the same in the complex plane. If x_3 is chosen so that γ is exactly one, the location of the zeroes coincide with those of the eigenvalues as indicated in the right graph of Fig. 7.1. This *pole-zero cancellation*, also demonstrated in [Jones 1996], means that for γ equal to one the suggested feedback controller would not move the eigenvalues at all.

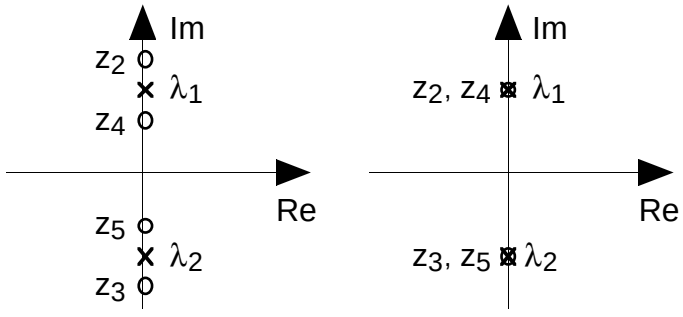

Fig. 7.1 Locations of oscillatory eigenvalues (x) and zeroes (o) for γ greater than one (left) and equal to one (right).

This agrees well with Chapter 3 and 4, which show that for the considered input and output signals, both controllability and observability of the inter-area mode are lost when γ is one. In the power system case, γ relates the *mass-scaled electrical distances* from the actuator to the machines. In order for the damping controller to be effective, it should be placed so that γ is far from one, as this moves the zeroes away from λ_1 and λ_2. Note that loss of mode observability and mode controllability both on their own will cause zeroes to coincide with the eigenvalues of the mode.

Although the locations of both zeroes and open-loop eigenvalues are determined as in Fig. 7.1, little can be said about the general shape of the root locus branches. This is clearly illustrated by Fig. 7.2. It shows the root locus of the spring-mass inter-area mode model for three values of M_1 while M_2, k_1 and k_2 are held constant.

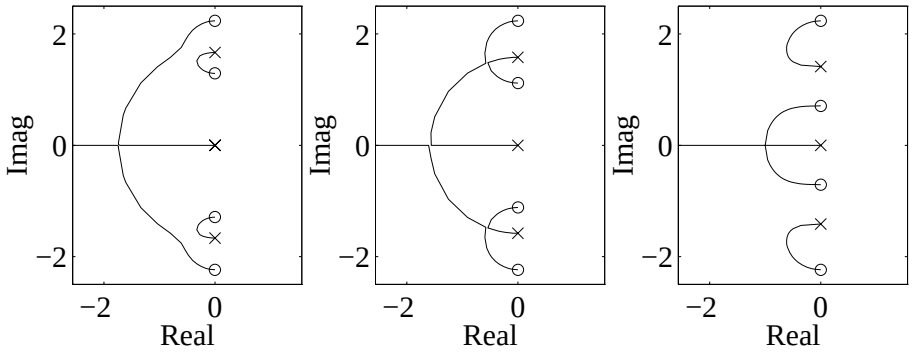

Fig. 7.2 Root locus of the spring-mass inter-area mode model with feedback from time derivative of x_3 to F_3. M_1 takes the values 3 (left), 4 (middle) and 10 (right) while k_1=5, k_2=10, M_2=2.

Zeroes for Feedback from Closest Machine Frequency

In the spring-mass inter-area mode model, the equivalent to closest machine frequency is v_1 if γ is greater than one and v_2 if γ is less than one. Without loss of generality, γ is assumed to be less than one in the following. The control law is consequently,

$$F_3 = d_3 v_2$$

which changes only a single element of (2.29) as,

$$diag\left(\begin{bmatrix} M_1 \\ M_2 \\ 1 \\ 1 \\ 0 \end{bmatrix}\right)\frac{d}{dt}\begin{bmatrix} v_1 \\ v_2 \\ x_1 \\ x_2 \\ x_3 \end{bmatrix} = \begin{bmatrix} 0 & 0 & -k_1 & 0 & k_1 \\ 0 & 0 & 0 & -k_2 & k_2 \\ 1 & 0 & 0 & 0 & 0 \\ 0 & 1 & 0 & 0 & 0 \\ 0 & -d_3 & k_1 & k_2 & -(k_1+k_2) \end{bmatrix}\begin{bmatrix} v_1 \\ v_2 \\ x_1 \\ x_2 \\ x_3 \end{bmatrix} + \begin{bmatrix} 1 & 0 \\ 0 & -1 \\ 0 & 0 \\ 0 & 0 \\ 0 & 0 \end{bmatrix}\begin{bmatrix} F_1 \\ F_2 \end{bmatrix} \quad (7.4)$$

Eliminating x_3 yields,

$$diag\left(\begin{bmatrix} M_1 \\ M_2 \\ 1 \\ 1 \end{bmatrix}\right)\frac{d}{dt}\begin{bmatrix} v_1 \\ v_2 \\ x_1 \\ x_2 \end{bmatrix} = \begin{bmatrix} 0 & -k_1\beta d_3 & -k_1\beta k_2 & k_1\beta k_2 \\ 0 & -k_2\beta d_3 & k_1\beta k_2 & -k_1\beta k_2 \\ 1 & 0 & 0 & 0 \\ 0 & 1 & 0 & 0 \end{bmatrix}\begin{bmatrix} v_1 \\ v_2 \\ x_1 \\ x_2 \end{bmatrix} + \begin{bmatrix} 1 & 0 \\ 0 & -1 \\ 0 & 0 \\ 0 & 0 \end{bmatrix}\begin{bmatrix} F_1 \\ F_2 \end{bmatrix} \quad (7.5)$$

where $\beta^{-1}=k_1+k_2$. By now letting the gain d_3 go to infinity, the resulting eigenvalues of the closed loop system are the zeroes of the open loop system. The feedback path from v_2 to its time derivative is made very fast and thus prevents deviations from zero in v_2. The corresponding eigenvalue is dominated by this path and yields the first zero,

$$z_1 \approx -\frac{k_2}{k_1+k_2}\frac{d_3}{M_2} \to -\infty$$

The state x_2 can be any constant value and will thus contribute to the system dynamics as an eigenvalue in the origin, giving

$$z_2 = 0$$

As v_2 is zero, so is its time derivative. From the second row of (7.4) it can then be concluded that x_3 will be constant, as it depends only on x_2 and F_2 that both are constants. A small part of (7.4) now describes the remaining dynamics,

$$diag\left(\begin{bmatrix} M_1 \\ 1 \end{bmatrix}\right)\frac{d}{dt}\begin{bmatrix} v_1 \\ x_1 \end{bmatrix} = \begin{bmatrix} 0 & -k_1 \\ 1 & 0 \end{bmatrix}\begin{bmatrix} v_1 \\ x_1 \end{bmatrix} + \begin{bmatrix} 1 & k_1 \\ 0 & 0 \end{bmatrix}\begin{bmatrix} F_1 \\ x_3 \end{bmatrix}$$

which yields two imaginary zeroes,

$$z_3 = z_4^* = j\sqrt{\frac{k_1}{M_1}}$$

For infinite gain the mass M_2 and the point described by x_3 are thus fixed and F_3 absorbs the forces caused by the swinging mass M_1. The resulting dynamics equals a part of that for infinite gain feedback from local bus frequency. It is therefore natural that z_3 and z_4 obtained here agree with z_2 and z_3 of (7.2). Again the zeroes can be compared to the eigenvalues λ_1 and λ_2. As γ is assumed to be less than one here, the oscillatory zeroes have a frequency less than that of the original inter-area mode, as shown in Fig. 7.3.

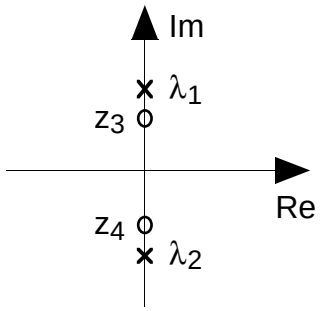

Fig. 7.3 Locations of oscillatory eigenvalues (x) and zeroes (o).

Again the rule of [Miu 1991] above applies, as the complex conjugate zeroes are the resonance frequencies of the substructure that can move, when the sensor and the actuator are fixed.

Remark: Equation (7.5) can be formulated as $\dot{x} = Ax + Bu$. The *trace* of *A* is obtained by summing the diagonal elements, which in this case yields the expression for z_1 above. The trace of *A* equals the sum of the eigenvalues, which for infinite gain is z_1. It can thus be concluded that the approximation of z_1 can be skipped making z_1 *equal* to the expression given.

7.2 Multi-Modal Decomposition

The modal description of the system with constant gain output feedback,

$$\dot{z} = [\Lambda + \Delta\Lambda]z = \left[\Lambda + \psi B_{ode}\left(I - KD_{ode}\right)^{-1} KC_{ode}\Phi\right]z \qquad (7.6)$$

also given as (2.10), shows that for large gains, the direct matrix D_{ode} needs to be taken into account. For the scalar control law *u=Ky* an infinite feedback gain *K* gives the eigenvalues and consequently the zero locations as,

$$\Lambda + \Delta\Lambda = \Lambda - \psi B_{ode} D_{ode}^{-1} C_{ode}\Phi \qquad (7.7)$$

where D_{ode} plays a central part. From (2.29) it can be realized that using local phase angle as measurement signal and active power as control signal yields a nonzero D_{ode}, since both input and output are algebraic variables related through an algebraic equation. As a lead filter also includes a direct term, the same applies for feedback from local bus frequency. On the other hand the frequency of the closest machine is a dynamic state. Therefore feedback from this signal to active power does not give rise to a direct matrix. But how can the zero locations be similar as in Fig. 7.1 and 7.3,

when D_{ode} is zero in one case and not in the other? The answer is that impact of other system modes is more important. A simplified, yet very powerful illustration to this is given in [Larsen et al 1995], where *Multi-Modal Decomposition* (*MMD*) as in Fig. 7.4 is applied.

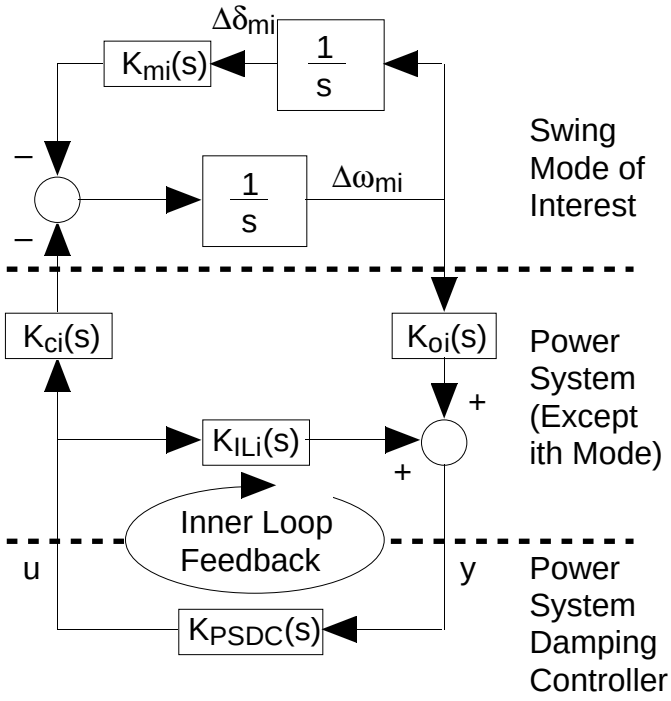

Fig. 7.4 Partial Multi-Modal Decomposition according to [Larsen et al 1995], with transfer function blocks $K_{ci}(s)$, $K_{oi}(s)$, $K_{mi}(s)$, $K_{ILi}(s)$ specifying the connections between inputs, outputs, velocity and angle of an electro-mechanical mode.

Mode *i* is then extracted and modelled as a modal system, connected to an input and an output via transfer functions $K_{ci}(s)$ and $K_{oi}(s)$ corresponding to the mode controllability and observability factors. The power system damping controller $K_{PSDC}(s)$ forms a feedback loop from the output to the input. The rest of the system is represented by a transfer function $K_{ILi}(s)$.

Together with the controller, $K_{ILi}(s)$ forms an *inner loop* that bypasses the dynamics of the mode to be damped. Transfer function zeroes occur at complex frequencies, for which $K_{ILi}(s)$ and the path via the modal system cancel each other. $K_{ILi}(s)$ thus largely determines the location of zeroes. As D_{ode} is only a (constant) part of $K_{ILi}(s)$ it only partly affects the zeroes.

The aim of the damping controller is to move the eigenvalues of mode *i*. If the mode is lightly damped and if its frequency and mode shape are not altered considerably by the control, the shift can be approximated according to [Larsen et al 1995],

$$\Delta\lambda_i \approx -\frac{1}{2} K_{ci} \left(I - K_{PSDC} K_{ILi}\right)^{-1} K_{PSDC} K_{ci} \qquad (7.8)$$

where all transfer functions are evaluated at $s=j\omega_i$; the eigenfrequency of λ_i. Note the resemblance between the matrix expression (7.6) and (7.8) using transfer functions.

From Fig. 7.4 it is obvious, that if the selected inputs and outputs are weakly related to mode *i*, then the inner loop will be relatively more important. This fact is particularly important for dampers that are located far away from the generators with both measurement signals and their actuator outputs indirectly related to the swing mode dynamics. This applies for the damping systems analysed above and for all FACTS dampers.

The existence of a nonzero K_{ILi} has two consequences: as discussed above, it limits the control authority by introducing zeroes. But it can also cause instability if,

$$K_{PSDC}(j\omega_i) K_{ILi}(j\omega_i) = I$$

In either case, feedback signal selection is critical since a good choice yields a small inner loop gain. To guarantee that a SISO system is robust to variations in K_{ILi}, the controller gain should be chosen so that

$$\left|K_{PSDC}(j\omega_i)\right|\left|K_{ILi}(j\omega_i)\right| GM = 1$$

where GM is a suitable gain margin [Larsen et al 1995]. If GM is sufficiently large, the parenthesized expression of (7.8) is approximately equal to unity. The eigenvalue shift due to this maximum gain is termed *Maximum Damping Index* (*MDI*) in [Larsen et al 1995] and is dominated by the controllability and observability factors K_{ci} and K_{oi} together with the controller.

When analyzing the joint operation of several damping controllers, K_{PSDC} and K_{ILi} are transfer function matrices. The stability limit is now described by,

$$\max\left|eig\left[K_{PSDC}(j\omega_i) K_{ILi}(j\omega_i)\right]\right| GM = 1$$

By searching the space spanned by the controller gains, GM may be maximized. The resulting gains and GM, can then be used for a multi-controller *MDI* which is described in [Othman et al 1995].

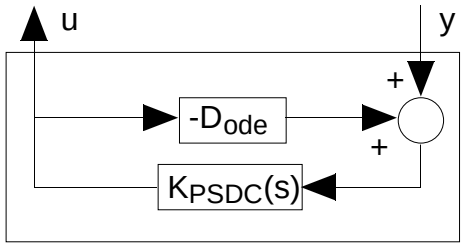

Fig. 7.5 Block diagram of a controller that cancels D_{ode}.

It may seem that the inner loop can be cancelled by compensating for it in the controller. As an example D_{ode} can be compensated for, if the controller $K_{PSDC}(s)$ is replaced by the control law in Fig. 7.5,

$$U(s) = \frac{K_{PSDC}(s)}{1 + K_{PSDC}(s) D_{ode}} Y(s)$$

where $U(s)$ and $Y(s)$ are the Laplace transforms of the input and the output signals. In the case when phase angle is measured, and the control signal is active power, the controller is a lead filter with a gain d_3 and a rather small time constant T ,

$$K_{PSDC}(s) = \frac{d_3 s}{1 + sT};\ D_{ode} = \frac{-1}{k_1 + k_2}$$

Inserting this into the control law above yields,

$$U(s) = \frac{\dfrac{d_3 s}{1 + sT}}{1 + \dfrac{d_3 s}{1 + sT} \dfrac{-1}{k_1 + k_2}} Y(s) = \frac{d_3 s}{1 - s\left(\dfrac{d_3}{k_1 + k_2} - T \right)} Y(s)$$

The eigenvalue of the controller will be positive already for small values of the gain d_3. As an unstable controller is not desired, compensation of D_{ode} is avoided.

7.3 Three Machine System

The suggested controllers are now numerically evaluated for the three machine system. The aim is to damp both oscillatory electro-mechanical modes with the active power injection of one damper. The magnitude information of Table 3.1 shows that bus N8 is the preferred location, even if bus N6 would yield slightly better controllability of the 1.8 Hz mode. The active power is controlled proportional to the local bus frequency or to the frequency of the closest machine.

Local Bus Frequency

Neither the spring-mass model nor the EUROSTAG models feature bus frequency as a natural state. Instead it is obtained by lead filtering a measurement of the phase angle at the bus. The transfer function of the resulting controller is,

$$\frac{P(s)}{\theta(s)} = K_d \frac{s}{1+s\tau} \tag{7.9}$$

where the time constant τ is set to 10 ms and K_d is the damper gain to be determined. This yields a phase advance of 85.4° at 1.3 Hz and 83.4° at 1.8 Hz, which is fairly close to the desired 90°.

According to (2.11), the eigenvalue sensitivity to the gain K_d can be obtained by multiplying the complex numbers for active power mode controllability and phase angle mode observability. In this case the controller has dynamics, and therefore the controller transfer function in (7.9) without K_d and evaluated at the mode frequency, is required as a third factor. The resulting numbers are given in Table 7.1, which indicates that in all cases the eigenvalues initially move almost straight to the left. The magnitude information supports the decision to place the damper at bus N8 with the very same reasoning as that based on controllability alone.

Bus	1.3 Hz mode	1.8 Hz mode
N5	$0.330e^{-j166°}$	$0.032e^{-j138°}$
N6	$0.239e^{-j164°}$	$0.327e^{-j168°}$
N8	$1.582e^{-j174°}$	$0.281e^{-j160°}$

Table 7.1 Eigenvalue sensitivity of the electro-mechanical eigenvalues in the second quadrant to local feedback from bus frequency to active power at the three load buses.

Introducing the controller at bus N8 and varying the gain yields the root locus of Fig. 7.6, which resembles that of the right graph of Fig. 7.2. The two oscillatory modes of the three machine system have zeroes with higher frequency and comparable damping when compared to the uncontrolled system eigenvalues. The behaviour of the spring-mass model inter-area mode thus agrees perfectly with both these modes. The third zero on the imaginary axis is a new electro-mechanical mode, replacing the rigid body mode. This is natural as the number of machines and modes are related: an *N* machine system has *N*-1 oscillatory modes. The introduction of the damper with infinite gain acts like a reference machine, thereby increasing the number of oscillatory modes by one.

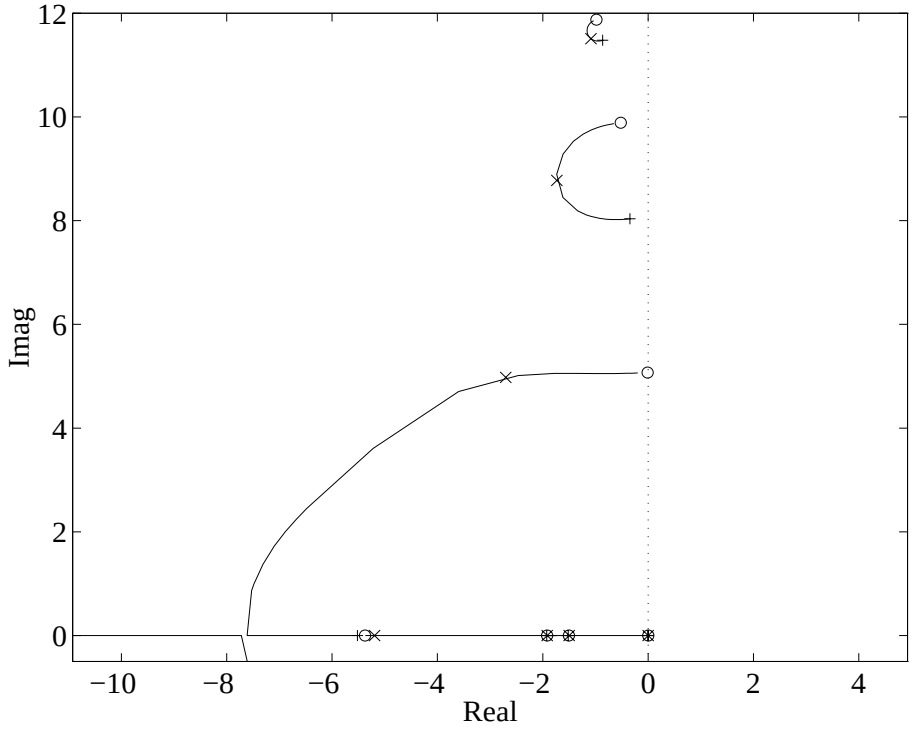

Fig. 7.6 Root locus for feedback from local frequency at bus N8 to active power injection at the same bus. Eigenvalue locations for the gains zero (+), 0.87 p.u./(rad/s) (x) and infinity (o) are indicated.

As predicted by the eigenvalue sensitivity measures, the 1.8 Hz mode is less influenced by the controller than the 1.3 Hz mode. Although both modes are damped, maximum damping does not occur for the same gain in both cases. The damping ability of the controller is best used by giving priority to the 1.3 Hz mode and maximize its damping by selecting the gain 0.87 p.u./(rad/s). This corresponds to 550 MW/Hz and the eigenvalues -1.1±j11.5, -1.7±j8.8 and -2.7±5.0 indicated by 'x' in Fig. 7.6.

Closest Machine Frequency

The active power injection at bus N8 will now be controlled by the rotor frequency of the closest machine. For the spring-mass model the control action and the measurement are then done on the same side of the *swing node*. This gives active power mode controllability and phase angle mode observability the same sign. For the three machine system this is demonstrated for each mode using the 3D-graphs of Figs 3.3 and 4.3. The mode observability of machine frequency is proportional to that of machine angle, which can be obtained by extrapolating the phase angle observability in the network beyond the machine terminals. This method indicates S2 and S3 as possible candidates for the 1.3 Hz mode while S3 and perhaps H1 can be used for the 1.8 Hz mode. Despite the uncertainty about the sign of the machine frequency controllability of H1 for the 1.8 Hz mode, it is clear that only S3 can be used for simultaneous damping of both modes.

A safer alternative is to use the exact observability information of Table 4.3. Combining this with the active power mode controllability at bus N8 in Table 3.1 gives the eigenvalue sensitivities of Table 7.2.

Machine	1.3 Hz mode	1.8 Hz mode
H1	$1.321e^{j2°}$	$0.093e^{j13°}$
S2	$3.902e^{-j175°}$	$0.917e^{-j3°}$
S3	$2.358e^{-j173°}$	$3.081e^{-j175°}$

Table 7.2 Eigenvalue sensitivity of the electro-mechanical eigenvalues in the second quadrant to feedback from machine frequency to active power at bus N8.

It is now evident that S3 is the only choice that will move the eigenvalues of both modes to the left. It also has the greatest impact on the 1.8 Hz mode and an acceptable influence on the 1.3 Hz mode, but this is less important than having the correct phase.

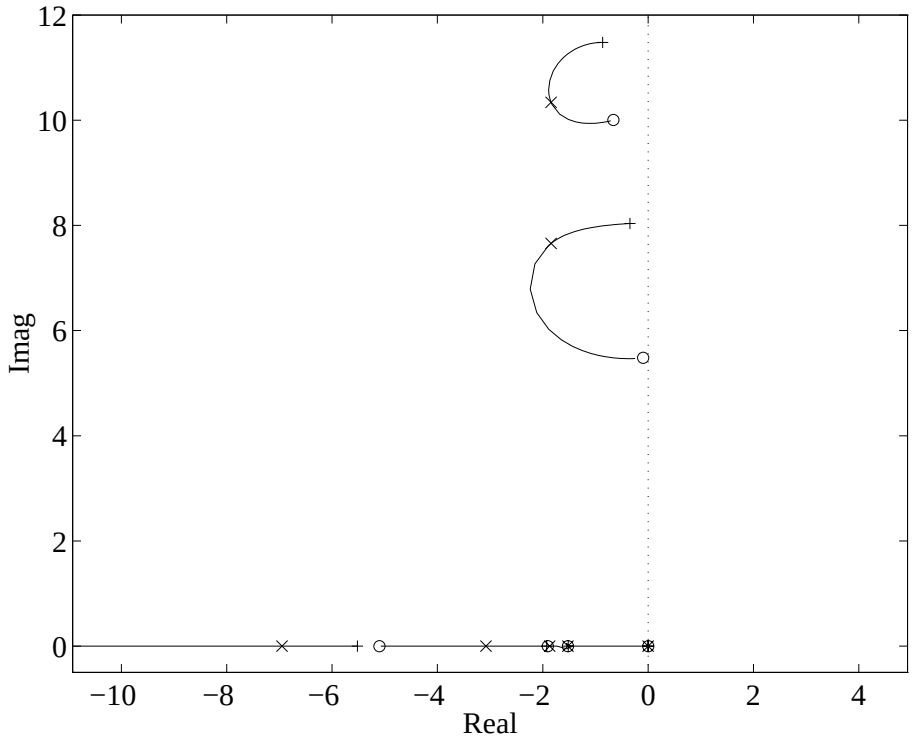

Fig. 7.7 Root locus for feedback from frequency of machine S3 to active power injection at bus N8. Eigenvalue locations for the gains zero (+), 0.5 p.u./(rad/s) (x) and infinity (o) are indicated.

Active power injected at bus N8 controlled by the rotor frequency of machine S3 gives the root locus of Fig. 7.7. Both the oscillatory modes move towards zeroes with low damping and lower frequency than the eigenvalues of the uncontrolled system. Just like for the bus frequency feedback case, both modes behave like the inter-area mode of the spring-mass model.

When increasing the gain from zero both the modes will be better damped. As the eigenvalue sensitivity of the 1.8 Hz mode to the feedback gain is greater than that of the 1.3 Hz mode, the 1.8 Hz mode reaches its point of maximum damping first. Close to this the real parts of both these eigenvalues are equal, which means that both modes have the same absolute damping. This point with gain 0.5 p.u./(rad/s) corresponding to 310 MW/Hz, is therefore considered the optimum one giving the eigenvalues -1.8±j7.7 and -1.8±j10.3, indicated by 'x' in Fig. 7.7.

It should be mentioned that both modes could be damped also if feedback were taken from S2. This however requires a compensation network that yields 180° phase shift between the two mode frequencies. Although possible, the simple gain suggested above is preferred due to its inherent *structural robustness* to changes in e.g. eigenfrequencies.

7.4 Twenty-three Machine System

Controlled active power injection at a load bus is now introduced in the twenty-three machine system. The main objective of the controller is to increase damping of the three least damped modes in the fault case when the double line N4044-N4045 is out. The selected modes in Table 2.2, are given priority in proportion to their need of additional damping.

Table 3.2 shows that the active power controllability of Mode 1 is greatest at bus N4072 followed by N63 and N4071. The External area including N4072 is however considered inaccessible and the damper is therefore placed at N63. It exhibits the greatest mode controllability of Mode 2 and is reasonably effective for Mode 3 as well.

The active power injection is controlled in proportion to the local frequency or to the frequency of the closest machine. Both cases are examined starting with local bus frequency.

Local Bus Frequency

Just like for the three machine system, the phase angle is measured and sent to the controller (7.9). The eigenvalue sensitivity to the gain K_d at each load bus can now be derived as in the previous section. It shows that local feedback from bus frequency to active power at any bus has either a beneficial or a negligible effect on damping of the three modes. At the buses with large sensitivity magnitude, the direction is close to the desired ±180°, and at buses with an argument between +90° and -90°, the magnitude is so small that the eigenvalue will not move far. Table 7.3 contains the results for the buses N51 and N63.

Bus	Mode 1	Mode 2	Mode 3
N51	$0.187e^{-j176°}$	$0.223e^{-j171°}$	$0.020e^{j22°}$
N63	$0.167e^{-j171°}$	$0.063e^{-j172°}$	$0.055e^{j175°}$

Table 7.3 Eigenvalue sensitivity of the selected eigenvalues in the second quadrant to local feedback from bus frequency to active power at the load buses N51 and N63.

Bus N51 is included as both Mode 1 and 2 are most sensitive to feedback there. This does not coincide with maximum active power mode controllability, which occurs at bus N63. The control signal magnitude of the damper at N63 may therefore differ from that at N51 if the two controllers are tuned for the same damping of these modes.

According to Table 7.3, Mode 3 will initially be *less damped* as the gain of the controller at N51 is increased from zero. This information can also be obtained from Fig. 3.5 together with Fig. 4.5: for Mode 3, the active power mode controllability and the phase angle mode observability have different signs at the buses N51, N4045 and N1045 respectively. In all other cases they have the same sign, corresponding to an initial leftward eigenvalue shift, when the gain of a local controller like (7.9) is increased from zero.

Bus N63 is chosen for its high controllability of Modes 1 and 2, but in order to explore the consequences of the inappropriate phase shift, bus N51 will also be studied. The root locus plots of Figs 7.8 and 7.9 show the eigenvalue locations for a varying controller gain K_d at the buses N51 and N63 respectively. The clutter at the real axis is due to the difficulty to trace the eigenvalues correctly and can be disregarded.

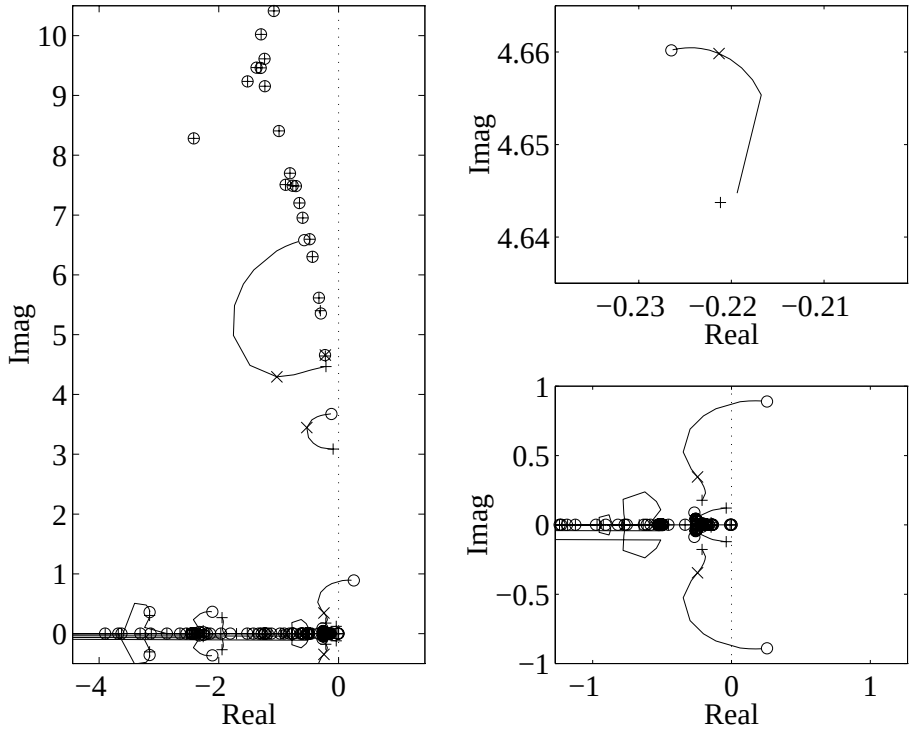

Fig. 7.8 Root locus for feedback from local frequency at bus N51 to active power injection at the same bus. Eigenvalue locations for the gains zero (+), 2.78 p.u./(rad/s) (x) and infinity (o) are indicated. The right graphs show details from the left plot: Mode 3 (upper) and rigid body mode (lower).

The eigenvalues of most electro-mechanical modes coincide with zeroes, indicating insignificant mode controllability or mode observability. Only three modes are considerably affected by the controllers. A slow complex mode goes unstable for sufficiently large gain, while Mode 1 and 2 move

via increased damping towards zeroes with higher frequency and relatively low damping.

According to the spring-mass model, the slow complex undamped zeroes form a new electro-mechanical mode that replaces the rigid body mode. The right eigenvectors of the unstable zeroes in Figs 7.8 and 7.9 in both cases exhibit the characteristics of a rigid body mode – the mechanical states of all machines are most active and move in unison. Note that the branches ending at the unstable zeroes have different origins in the two cases. The rigid body zeroes thus need *not* originate in the open-loop rigid body mode.

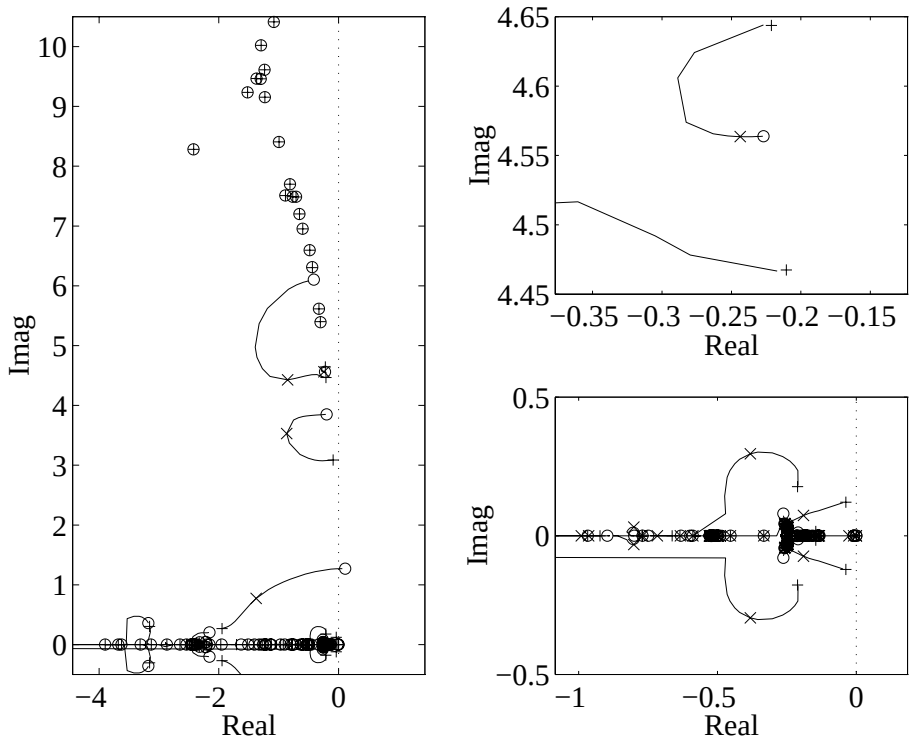

Fig. 7.9 Root locus for feedback from local frequency at bus N63 to active power injection at the same bus. Eigenvalue locations for the gains zero (+), 4 p.u./(rad/s) (x) and infinity (o) are indicated. The right graphs show details from the left plot: Mode 3 (upper) and rigid body mode (lower).

In Fig. 7.8 the eigenvalues of Mode 3 move to the right as predicted. Before reaching very far, they are however attracted by nearby zeroes with higher frequency and higher damping. Mode 3 is thus practically unaltered and can be disregarded when selecting the gain. This is instead a compromise between damping of Mode 1 and 2. As Mode 1 should be given priority, it is natural to maximize its damping.

For the N51 case the gain 2.78 p.u./(rad/s) or 1750 MW/Hz moves Mode 1 to -0.5±j3.4 and Mode 2 to -1.0±j4.3 which is indicated by 'x' in Fig. 7.8. The damping of Mode 3 is unaltered just like that of the eigenvalues passing the imaginary axis for large gains.

With the damper at N63 the optimum gain is chosen as 4 p.u./(rad/s) or 2500 MW/Hz, which places Mode 1 at -0.9±j3.5 and Mode 2 at -0.85±j4.4 (indicated by 'x' in Fig. 7.9) while the damping of Mode 3 is slightly improved. The eigenvalues moving towards the unstable zeroes have come closer to the imaginary axis, but are still well damped.

It is important to realize that when the eigenvalues are shifted as in Figs 7.8 and 7.9, the eigenvectors are also affected. Fig. 7.10 illustrates the complex values of the active power mode controllability at the load buses, for the gains d_{51}=2.78 and d_{63}=4 p.u./(rad/s) respectively.

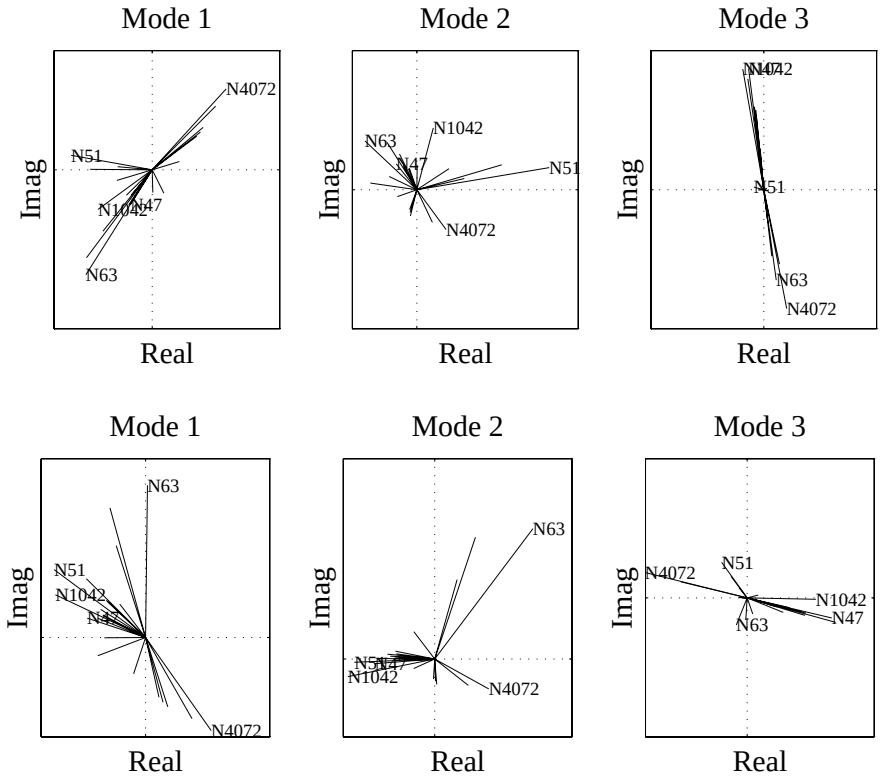

Fig. 7.10 Complex active power mode controllability at the load buses when one damper is in use. For the upper graphs the damper location is bus N51 with gain d_{51}=2.78 p.u./(rad/s), while for the lower graphs the location is bus N63 and the gain d_{63} is 4 p.u./(rad/s).

Comparing Fig. 7.10 to the situation with no dampers in Fig. 3.4, shows that the damper has a strong effect on the argument of the eigenvector elements. It is clear that the eigenvectors of Modes 1 and 2 are affected the most, which is expected as it was the corresponding eigenvalues that

received the most additional damping. The same applies for the complex phase angle mode observability at the load buses, shown without dampers in Fig. 4.4 and in Fig. 7.11 for the two single damper cases above.

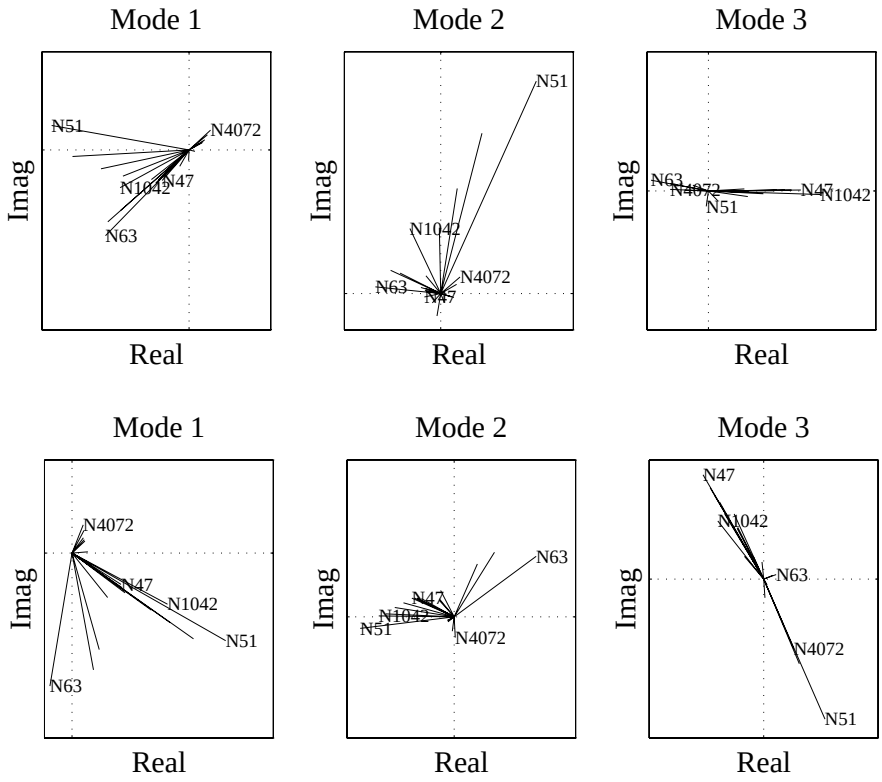

Fig. 7.11 Complex phase angle mode observability at the load buses when one damper is in use. For the upper graphs the damper location is bus N51 with gain d_{51}=2.78 p.u./(rad/s), while for the lower graphs the location is bus N63 and the gain d_{63} is 4 p.u./(rad/s).

Due to the greater variation in arguments it is now impossible to fit a straight line to the controllability values as in Fig. 3.4 or to the observability values as in Fig. 4.4. The 3D-visualization of active power mode controllability and phase angle mode observability used in Chapters 3 and 4 can therefore now only be applied to Mode 3, that is practically unaffected by the two suggested dampers.

Closest Machine Frequency

For loads that are directly or radially connected to a machine bus, the active power controllability of all modes is similar at the load and at the machine. The identification of the closest machine is therefore trivial at the load buses N1012, N1013, N1022, N1042, N1043, N2032, N4071, N4072, N41, N42, N47, N51, N62 and N63. The machine closest to bus N63 is thus A4063.

Fig. 2.9a also indicates that the machine frequency observability of Mode 1 and 2 is greatest at A4051. This agrees well with the large bus frequency observability at bus N51 and may even compensate for the lower active power controllability there. Active power injection at bus N51 controlled by the machine frequency of A4051 is therefore considered along with the combination of N63 and A4063. To start with, the frequency signals are taken from machine 1 at each plant.

Table 7.4 shows the eigenvalue sensitivity of the selected modes to the two feedback alternatives. Indeed both Mode 1 and 2 are more sensitive to the control of active power at bus N51 than at bus N63. On the other hand, Mode 3 exhibits a rightward direction like in the local bus frequency case.

Bus	Machine	Mode 1	Mode 2	Mode 3
N51	A4051_1	$0.265e^{-j178°}$	$0.395e^{-j174°}$	$0.040e^{j19°}$
N63	A4063_1	$0.236e^{-j173°}$	$0.152e^{-j170°}$	$0.117e^{j173°}$

Table 7.4 Eigenvalue sensitivity of the selected eigenvalues in the second quadrant to feedback from ω_{A4051_1} and ω_{A4063_1} to active power injection at bus N51 and N63 respectively.

The root locus plots resulting from a gain variation in each case are given as Figs 7.12 and 7.13. Again the controller substantially influences only three modes, while most of the electro-mechanical modes are cancelled by zeroes. Two of the selected modes are damped, while another mode moves towards a pair of complex unstable zeroes just like in Figs 7.8 and 7.9. Whereas the achievable damping of one mode is comparable to that in the bus frequency case, the other one can be almost completely damped.

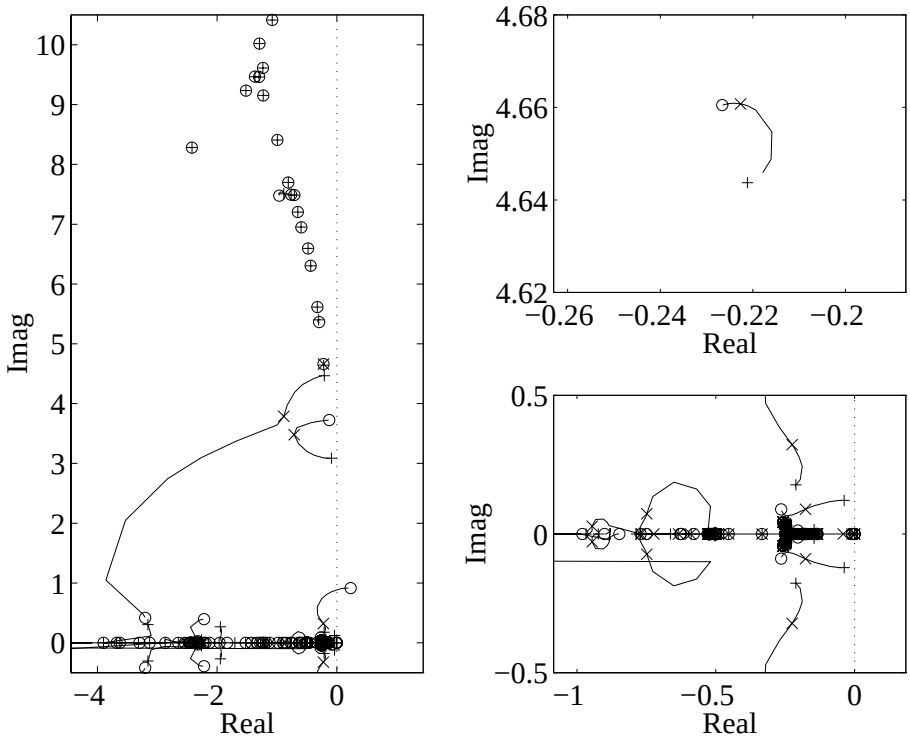

Fig. 7.12 Root locus for feedback from rotor angular velocity of A4051_1 to active power injection at bus N51. Eigenvalue locations for the gains zero (+), 2.4 p.u./(rad/s) (x) and infinity (o) are indicated. The right graphs show details of Mode 3 (upper) and the origin (lower).

Although the locations of zeroes are very similar in Figs 7.12 and 7.13, the resulting plots are different and look like the left and right graphs of Fig. 7.2. For active power injection at bus N51, the maximum damping of Mode 1 is limited while that of Mode 2 is very high. The location N63 gives the opposite result. This difference in damping ability was not seen when using bus frequency for feedback. A possible explanation is that Modes 1 and 2 change identities as their branches come very close in Fig. 7.12. A similar phenomenon is reported in [Klein et al 1992]: measures based on eigenvectors are incorrect when two eigenvalues are close. Due to the uncertainty about who is who of the two modes, they will be addressed as the *fast* and *slow* study mode.

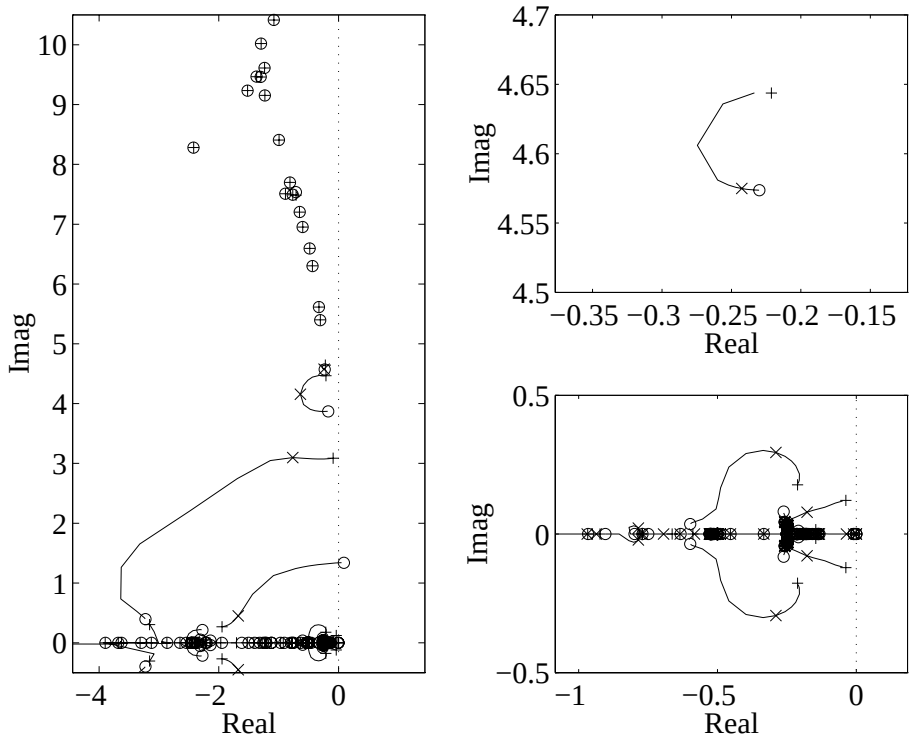

Fig. 7.13 Root locus for feedback from rotor angular velocity of the machine A4063_1 to active power injection at bus N63. Eigenvalue locations for the gains zero (+), 2.6 p.u./(rad/s) (x) and infinity (o) are indicated. The right graphs show details of Mode 3 (upper) and the origin (lower).

Mode 3 initially moves to the right in Fig. 7.12, but in both cases it is practically uncontrollable. The gain selection is therefore based on the two first modes. The gain for active power at bus N51 controlled by the rotor angular velocity of the machine A4051_1 is set to 2.4 p.u./(rad/s) or 1500 MW/Hz, which yields maximum damping of the slow study mode (-0.7±j3.5) and even better damping of the fast one (-0.9±j3.8) as indicated by 'x' in Fig. 7.12. The optimum gain for controlling active power at bus N63 is 2.6 p.u./(rad/s) or 1600 MW/Hz. This maximizes the damping of the fast study mode (-0.6±j4.2), while that of the slow study mode is slightly better (0.8±j3.1) as indicated by 'x' in Fig. 7.13.

The eigenvalue shifts achieved above again implicate a change in the eigenvectors. The active power mode controllability at the load buses is shown in Fig. 7.14 for the gains d_{51}=2.4 and d_{63}=2.6 p.u./(rad/s).

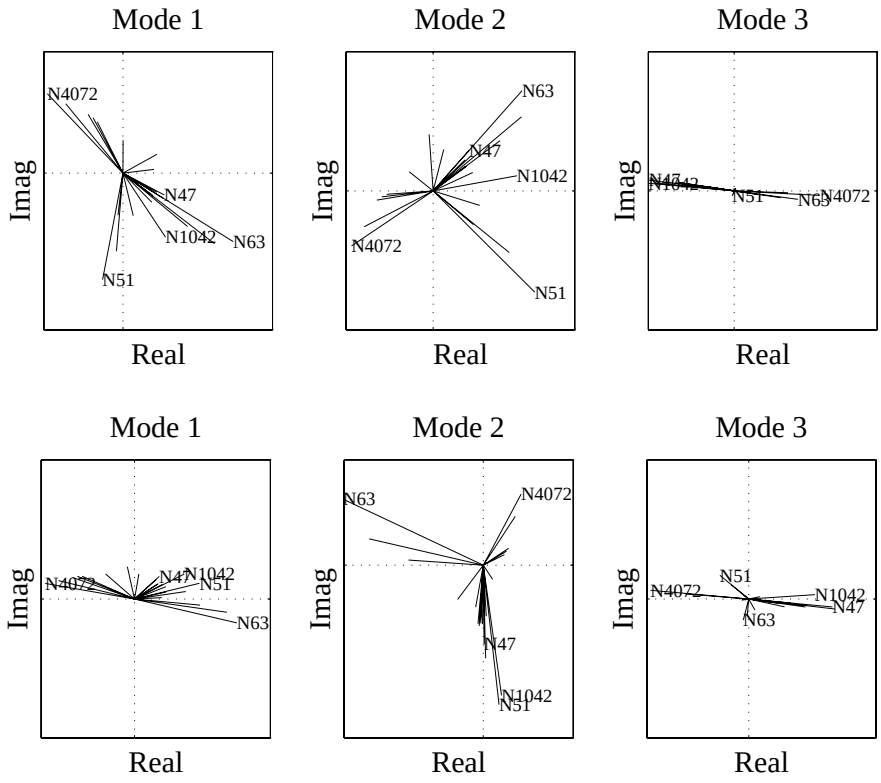

Fig. 7.14 Complex active power mode controllability at the load buses when one damper is in use. For the upper graphs the damper location is bus N51 with gain d_{51}=2.4 p.u./(rad/s), while for the lower graphs the location is bus N63 and the gain d_{63} is 2.6 p.u./(rad/s).

The machine frequency mode observability, which resembles the mode shape, is shown in Fig. 7.15 for the cases when d_{51}=2.4 or d_{63}=2.6 p.u./(rad/s). Modes 1 and 2 again experience a great variation in arguments as compared to Figs 3.4 and 4.4 that show the corresponding values when no damper is present.

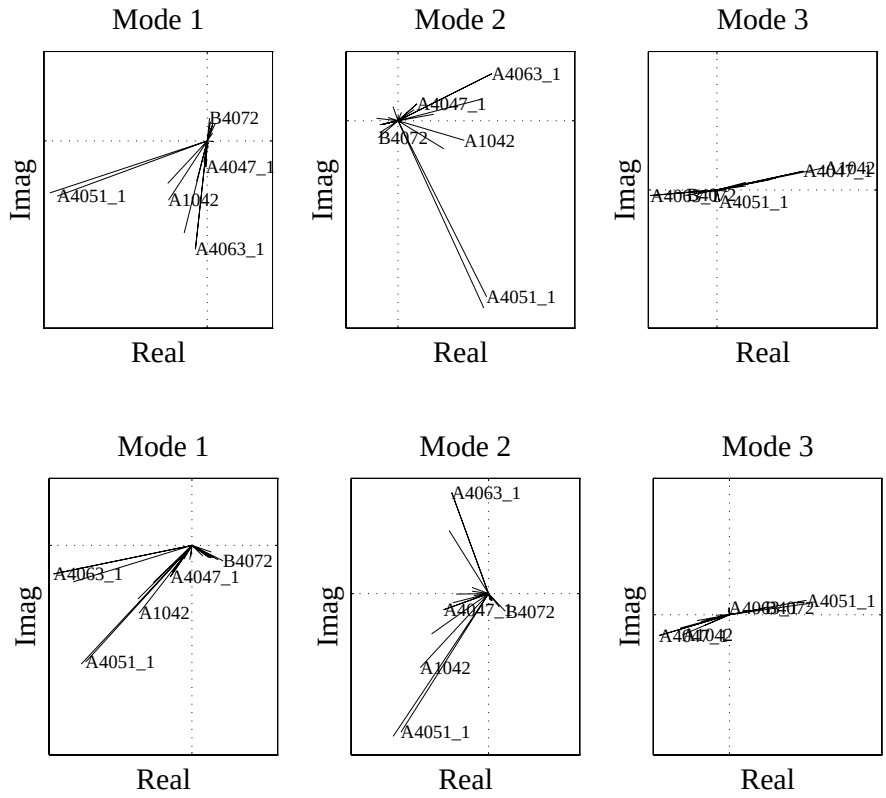

Fig. 7.15 Complex mode observability for machine frequency when one damper is in use. For the upper graphs the damper location is bus N51 with gain d_{51}=2.4 p.u./(rad/s), while for the lower graphs the location is bus N63 and the gain d_{63} is 2.58 p.u./(rad/s).

Selecting d_{51}=2.4 p.u./(rad/s) places the eigenvalues of Modes 1 and 2 fairly close to each other and it is clear from Fig. 7.12 that the root locus branches are attracted to each other. The upper parts of Figs 7.14 and 7.15 indicate that the eigenvectors of the two modes are quite similar. As the modes are identified by their eigenvectors, it is hard to tell them apart at this point. This observation supports the assumption above that Modes 1 and 2 actually change identities with each other for a value of d_{51} close to 2.4.

An alternative to using the rotor velocity of *one* machine at a power station is the average velocity of *both* machines. However, this has no effect on the results given here, as the operating points of machine 1 and 2 are completely or almost identical. For all electro-mechanical modes except the local mode, the two machines then operate as one of twice the size. But the local mode, where they swing against each other, is not controllable with active power injection in the network.

7.5 Conclusions

Controlling active power at one bus in proportion to the local bus frequency or the frequency of the closest machine can increase damping of more than one mode, while leaving other modes unaffected. Damping is however limited as the eigenvalues tend towards zeroes with low damping. The locations of these zeroes relative to the open-loop eigenvalues are qualitatively the same for the inter-area mode of the spring-mass model as for the electro-mechanical modes of the multi-machine power systems. In both cases rigid body zeroes with little or even negative damping arise.

No certain statements can be made about the shape of the root locus. If the modes are sufficiently far from each other in the complex plane, the branches are in general semi-circular. The same shape is observed, when changing the parameters of a load model where the active power depends dynamically on the voltage [Hiskens and Milanovic 1995]. If instead both eigenvalues and eigenvector shapes are sufficiently close the branches interact. A consequence of this is that modes may change identities even if their branches do not meet. This is observed for Modes 1 and 2 in Fig. 7.12, but also explains the fact that the unstable zeroes represent a rigid body mode even if the branches leading to them do not originate in the rigid body mode eigenvalues of the open loop system.

The impact of zeroes on the damping of a mode is reduced as the measurement signal is closer related to a machine that participates strongly in the mode. Mode 1 and 2 are dominated by the machines A4063 and A4051 respectively. Placing the controller close to A4063 will therefore promote damping of Mode 1 rather than Mode 2, while the opposite applies for a location at A4051.

Gains are chosen for maximum damping of either Mode 1 or 2 and reasonable damping of the other one, even if acceptable damping is obtained already at much lower gains. This gives values of 1250-2500 MW/Hz which agrees well with the gains suggested on page 143 in [Smed 1993] for the damping controller of the Fenno-Skan HVDC link. The gains can also be compared to the characteristics of the NORDIC32 system [CIGRÉ 1995]: the frequency sensitivity of the loads is 165 MW/Hz and the total frequency control gain of 4375 MW/Hz at steady state.